INTERNATIONAL JOURNAL FOR NUMERICAL METHODS IN FLUIDS, VOL. 27, 127–138 (1998)

SIMULATION OF STEADY COMPRESSIBLE FLOWS BASED ON CAUCHY/RIEMANN EQUATIONS AND CROCCO'S RELATION

M. HAFEZ* AND W. H. GUO

Department of Mechanical and Aeronautical Engineering, University of California, Davis, CA 95616, U.S.A.

SUMMARY

In this paper, alternative formulations of the steady Euler equations for conservation of mass, momentum and energy are adopted for the numerical simulation of compressible flows with shock waves. The total enthalpy is assumed to be constant and hence an isentropic density is calculated in terms of the velocity components. Also, the x- and y-momentum equations written in conservation form are combined to yield the tangential and normal momentum equations. For smooth flows the tangential momentum equation reduces to the entropy transport equation, while the normal momentum equation gives the vorticity in terms of the entropy gradient normal to the flow direction (Crocco's relation). Hence the velocity components can be obtained from the continuity equation and normal momentum equation (Cauchy/Riemann equations), while the entropy correction for the density is obtained from the tangential momentum equation (this correction is not needed in the isentropic flow regions). The present formulation can be easily extended to handle variable total enthalpy. Preliminary results are presented for transonic and supersonic flows over aerofoils and the entropy and vorticity effects are clearly identified. © 1998 John Wiley & Sons, Ltd.

Int. J. Numer. Meth. Fluids, **27**: 127–138 (1998)

KEY WORDS: compressible flow; supersonic flows; aerofoils; Cauchy/Riemann equations; Crocco's relation

1. INTRODUCTION

In the last two decades, intensive efforts have been directed to the solution of the Euler equations in conservation form, with great success (see e.g. References 1 and 2). One can argue, however, that for most external aerodynamic applications in the transonic and supersonic regimes the inviscid flow is mainly isentropic and irrotational, except for regimes behind curved shocks. Therefore it is desirable to identify entropy and vorticity effects and to calculate them only in the regions where they do not vanish. Hopefully such a strategy will lead to more efficient and accurate calculations. The main idea is to decouple the acoustics from entropy and vorticity modes. One way to achieve this goal is to detect the shock location and slope and explicitly impose the entropy jump across the shock as an internal boundary condition for the flow downstream of the shock. Algorithms based on this approach have been developed by the first author in References 3 and 4. Recent calculations using entropy, a modified density and velocity components as dependent variables are presented in the Appendix following the work of Tang and Hafez.[5] The shock detection problem, however, may require

* Correspondence to: M. Hafez, Department of Mechanical and Aeronautical Engineering, University of California, Davis, CA 95616, U.S.A.

CCC 0271–2091/98/010127–12 $17.50 *Received May 1996*

complicated logic, particularly for three-dimensional flows.

Other algorithms with shocks automatically captured are proposed by Paillere *et al.*[6] and Ta'asan.[7] The motivation in Reference 6 is to construct a genuinely multidimensional upwinding scheme. This can be accomplished at least for the scalar entropy and total enthalpy equations. Local transformation is then used to obtain the solution in terms of the conservative variables. The motivation in Reference 7 is to implement multigrid efficiently to solve the Euler equations for steady compressible flows. However, only subsonic flow results have been presented, and since staggered grids are used, a discrete potential exists and fast convergence is expected for such an elliptic system.

In the present work an alternative formulation based on the Cauchy/Riemann equations and Crocco's relation is adopted. A modified density in terms of the velocity components and total enthalpy is introduced with an entropy correction calculated from the tangential momentum equation. The velocity components are obtained from the continuity and normal momentum equations assuming the entropy is known and the process is repeated until convergence.

For isentropic, irrotational flows, only the Cauchy/Riemann equations are solved for the velocity components with density obtained from Bernoulli's law. This subset is valid, for example, in the far field where the flow is smooth or shock waves are weak.

The present formulation can be numerically implemented using a finite element/finite volume discretization procedure and a balanced artificial viscosity discussed in Reference 4. For convenience a simplified version of this procedure for regular grids is used here. With small artificial viscosity coefficients, pseudo-time-dependent terms are added to the equations to enhance the diagonal dominance of the algebraic equations. A line relaxation procedure with a 2×2 block tridiagonal solver is used to solve the linearized equations for the velocity components and a scalar tridiagonal solver is used for the entropy correction.

Preliminary results are presented for transonic and supersonic flows over aerofoils. The formulation is tested first for a quasi-one-dimensional supersonic flow in a divergent nozzle and for a two-dimensional shock reflection problem.

2. PROBLEM FORMULATION

To demonstrate the feasibility of the present formulation, a supersonic flow with a shock wave in a divergent nozzle is studied. The quasi-one-dimensional Euler equations can be written in the form

$$(\rho u A)_x = 0, \tag{1}$$

$$(\rho u^2 A)_x + (Ap)_x = A_x p, \tag{2}$$

$$\frac{\gamma}{\gamma - 1}\frac{p}{\rho} + \tfrac{1}{2}u^2 = H = \frac{\gamma + 1}{2(\gamma - 1)}. \tag{3}$$

Let us introduce the variables ρ_i and p_i such that

$$\rho = \rho_i E \quad \text{and} \quad p = p_i E, \tag{4}$$

where

$$E = \mathrm{e}^{-\Delta s/R};$$

also

$$p_i = \rho_i^{\gamma}/\gamma. \tag{5}$$

It is clear then that ρ_i can be obtained from Bernoulli's law (equation (3)) and equations (1) and (2) can be solved for u and E. In other words, the speed and entropy are updated to satisfy the continuity and momentum equations respectively.

For two-dimensional flows the standard governing equations are

$$(\rho u)_x + (\rho v)_y = 0, \tag{6}$$

$$(\rho u^2)_x + (\rho uv)_y + p_x = 0, \tag{7}$$

$$(\rho uv)_x + (\rho v^2)_y + p_y = 0, \tag{8}$$

$$\frac{\gamma}{\gamma - 1}\frac{p}{\rho} + \tfrac{1}{2}(u^2 + v^2) = \frac{1}{\gamma - 1}\frac{1}{M_\infty^2} + \tfrac{1}{2}. \tag{9}$$

With the tangency condition at solid surfaces and proper far-field behaviour, one can obtain a solution of the above system of equations.

Here the x- and y-momentum equations (7) and (8) are combined to produce the normal and tangential momentum equations, namely

$$u[(\rho uv)_x + (\rho v^2)_y + p_y] - v[(\rho u^2)_x + (\rho uv)_y + p_x] = 0, \tag{10}$$

$$u[(\rho u^2)_x + (\rho uv)_y + p_x] + v[(\rho uv)_x + (\rho v^2)_y + p_y] = 0. \tag{11}$$

For smooth flows, equation (10) reduces to

$$-u_y + v_x = \frac{p}{\rho q}\left(\frac{u}{q}\frac{\partial(\Delta s/R)}{\partial y} - \frac{v}{q}\frac{\partial(\Delta s/R)}{\partial x}\right), \tag{10a}$$

while equation (11) becomes

$$\left(\rho u\frac{\Delta s}{R}\right)_x + \left(\rho v\frac{\Delta s}{R}\right)_y = 0. \tag{11a}$$

Introducing the variables ρ_i and p_i defined by (4), where p_i is proportional to ρ_i^γ, Bernoulli's law (equation (9)) provides a formula for ρ_i in terms of the speed:

$$\rho_i = \left(1 - \frac{\gamma - 1}{2}M_\infty^2(u^2 + v^2 - 1)\right)^{1/(\gamma-1)}. \tag{12}$$

Assuming the entropy is known, equations (6) and (10) are solved to obtain u and v. It is important to account properly for the non-linearity of these equations; in particular, the dependence of ρ_i on u and v is responsible for their mixed-type (hyperbolic/elliptic) nature. It is also interesting to notice that this system has the same form of characteristics as the irrotational, isentropic flow equations. The entropy function E is then updated from (11) and the process is repeated until convergence.

In the smooth flow regions, equations (10) and (11) can be replaced by equations (10a) and (11a). However, the latter are not valid across shocks. Entropy is generated across a shock wave to satisfy the momentum equations. Equation (10a) relates the vorticity to the variation in entropy from one streamline to another, while equation (11) implies that entropy is constant along a streamline.

If the total enthalpy is not constant everywhere, the energy equation for adiabatic flows implies that H must be constant along a streamline, i.e.

$$(\rho uH)_x + (\rho vH)_y = 0. \tag{13}$$

This scalar equation must be solved, with the given inlet condition, to obtain the distribution of H. In this case, ρ_i is calculated from the equation

$$\rho_i = \{(\gamma - 1)M_\infty^2[H - \tfrac{1}{2}(u^2 + v^2)]\}^{1/(\gamma-1)}. \tag{14}$$

Equation (10) will also be modified to read

$$-u_y + v_x = \frac{p}{\rho q}\left(\frac{u}{q}\frac{\partial(\Delta s/R)}{\partial y} - \frac{v}{q}\frac{\partial(\Delta s/R)}{\partial x}\right) - \frac{1}{q}\left(\frac{u}{q}\frac{\partial H}{\partial y} - \frac{v}{q}\frac{\partial H}{\partial x}\right). \tag{15}$$

In the following the numerical results of some preliminary calculations are discussed.

3. NUMERICAL RESULTS

3.1. Nozzle flow

Consider supersonic flow in a divergent nozzle. The parameters at the throat of the nozzle are $\rho^* = 1$, $u^* = 1$, $M^* = 1$, $A^* = 1$ and $p^* = 1/\gamma = 0{\cdot}714$. The exit pressure p_e is 1·018. The grid consists of 121 points.

The convergence history and numerical results are shown in Figure 1. The shock location is identified with the maximum entropy increase ($(\Delta s/R)_{\max}$). The numerical results are in good agreement with the exact solution.

3.2. Parabolic arc aerofoil at $\tau = 0{\cdot}1$ in subsonic flow

To test the two-dimensional programme, subsonic flow at $M_\infty = 0{\cdot}5$ is calculated over a thin aerofoil with and without the entropy corrections. Figure 2(a) shows the Mach number contours and Figure 2(b) gives the C_p distributions in both cases. As expected, the two results are almost identical.

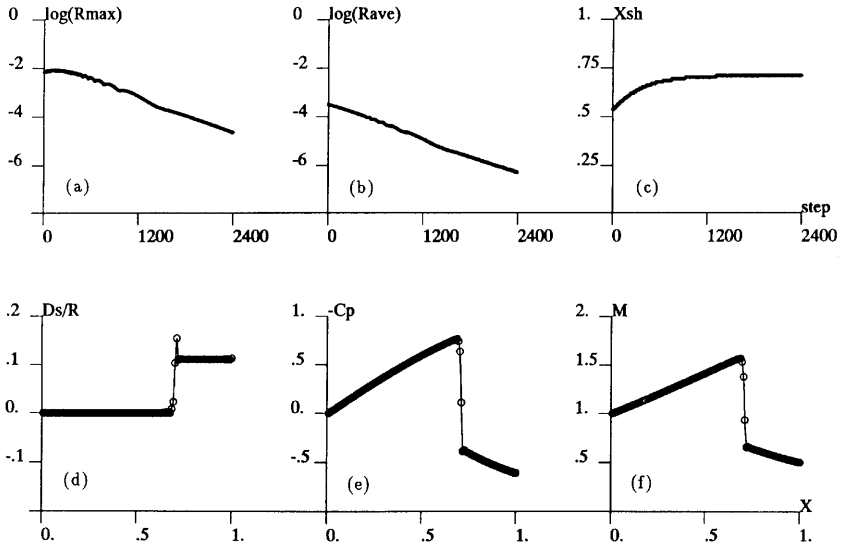

Figure 1. Nozzle ($p_e = 1{\cdot}018$) convergence history and results: (a) $R_{\max} = (\Delta\rho)_{\max}$; (b) R_{ave}, average values of $\Delta\rho$; (c) location of shock; (d) entropy distribution; (e) C_p distribution; (f) Mach number distribution

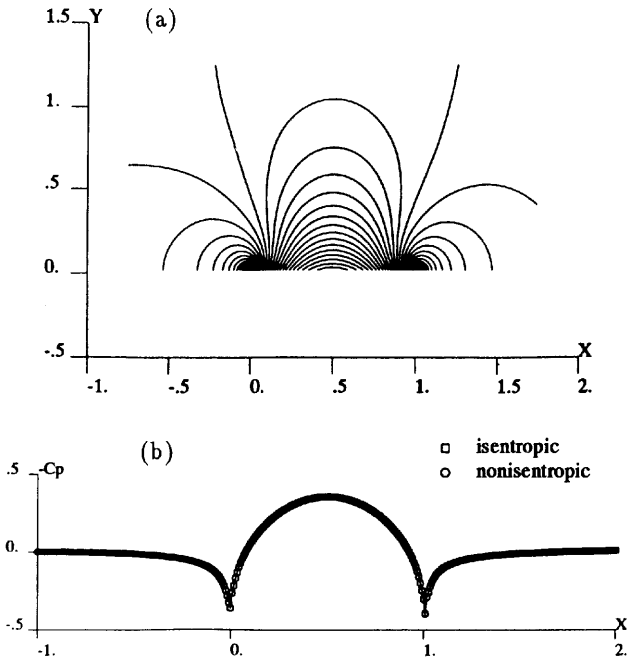

Figure 2. Parabolic arc aerofoil ($\tau = 0{\cdot}1$, $M_\infty = 0{\cdot}5$): (a) Mach number contours; (b) C_p distributions with and without entropy correction

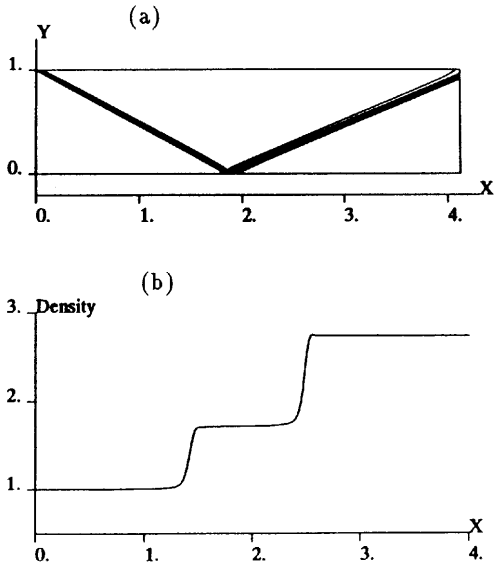

Figure 3. Shock reflection ($M_\infty = 2{\cdot}9$): (a) pressure contours; (b) density at $y = 0{\cdot}25$

3.3. *Shock reflection in supersonic flow*

In this example a shock is formed from the leading edge of a wedge at $\delta = 10{\cdot}93^\circ$. The incoming flow Mach number is 2·9. The pressure contours and density distribution at $y = 0{\cdot}25$ are presented in Figure 3. Again the numerical results are in agreement with the exact solution.

3.4. *Parabolic arc aerofoil at* $\tau = 0{\cdot}2$ *in transonic flow*

Transonic flow passing the parabolic arc aerofoil is calculated for $M = 0{\cdot}8$. Figure 4(a) gives the C_p distributions for both isentropic and non-isentropic cases. It is shown that the shock moves upstream and becomes weaker if entropy correction is accounted for. The entropy contours are shown in Figure 4(b). Figures 4(c) and 4(d) give a comparison of the pressure contours of both cases.

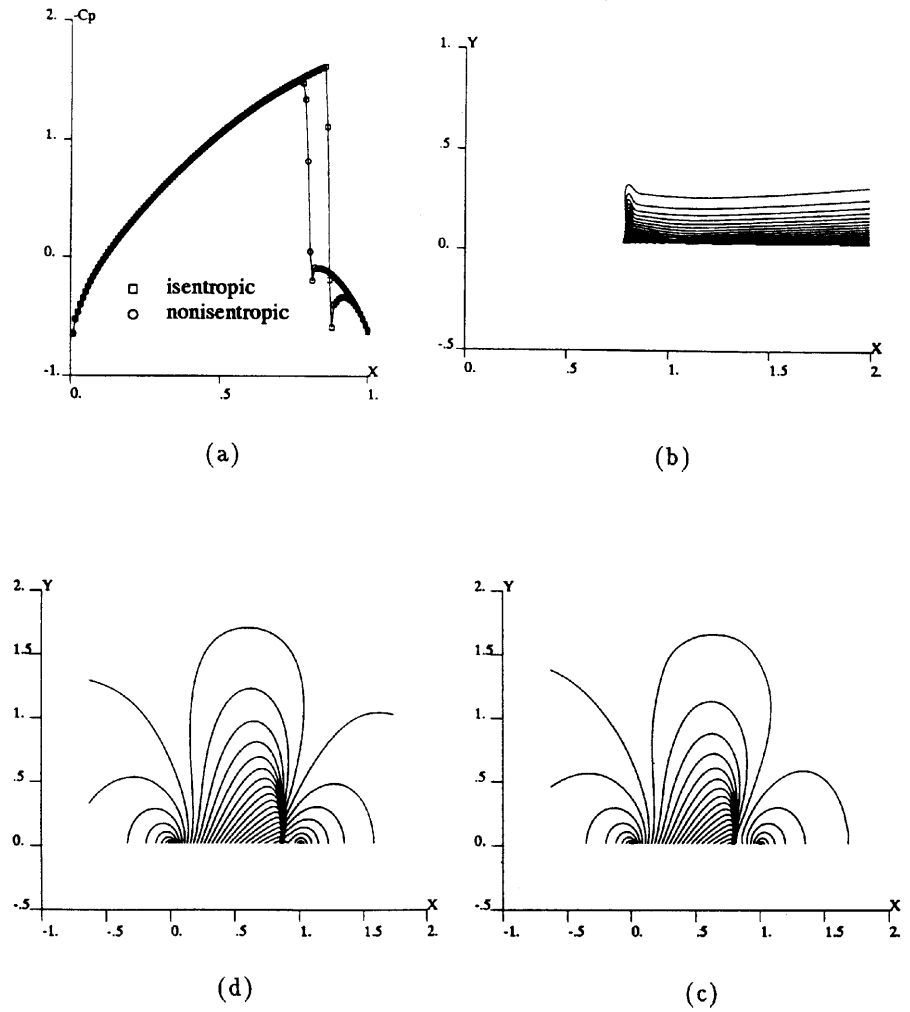

Figure 4. Parabolic arc aerofoil ($\tau = 0{\cdot}2$, $M_\infty = 0{\cdot}8$): (a) C_p distributions; (b) entropy contours; (c) pressure contours for non-isentropic flow; (d) pressure contours for isentropic flow

3.5. NACA 0012 aerofoil in transonic flow

Another transonic problem is calculated for flow passing an NACA 0012 aerofoil at $M_\infty = 0{\cdot}85$. Figure 5 shows the corresponding results.

3.6. NACA 0012 aerofoil in supersonic flow

For a freestream Mach number of 1·4 a bow shock is formed near the leading edge and an oblique shock is formed at the trailing edge. The bow shock moves upstream and becomes weaker for non-isentropic flow. The numerical results are shown in Figure 6. Similar results were obtained for another example with a freestream Mach number of 1·6 where the shock is stronger (Figure 7).

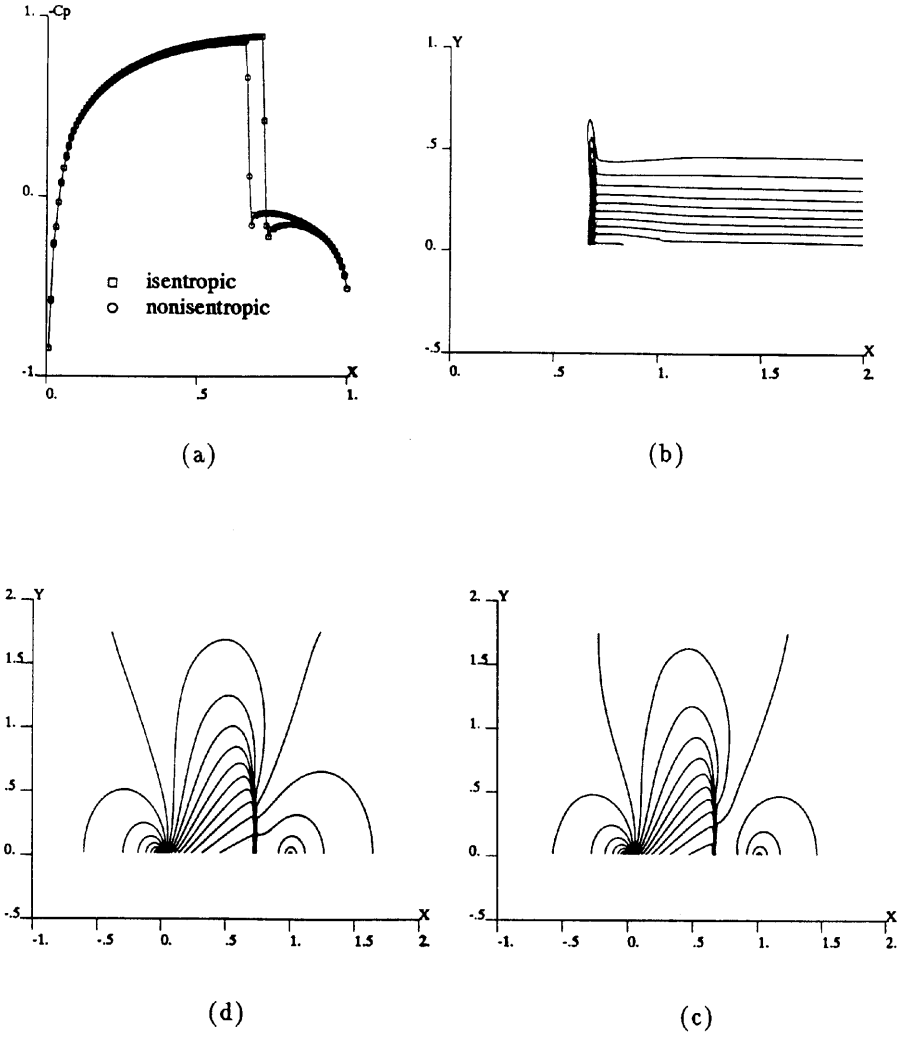

Figure 5. NACA 0012 aerofoil ($M_\infty = 0{\cdot}85$): (a) C_p distributions; (b) entropy contours; (c) pressure contours for non-isentropic flow; (d) pressure contours for isentropic flow

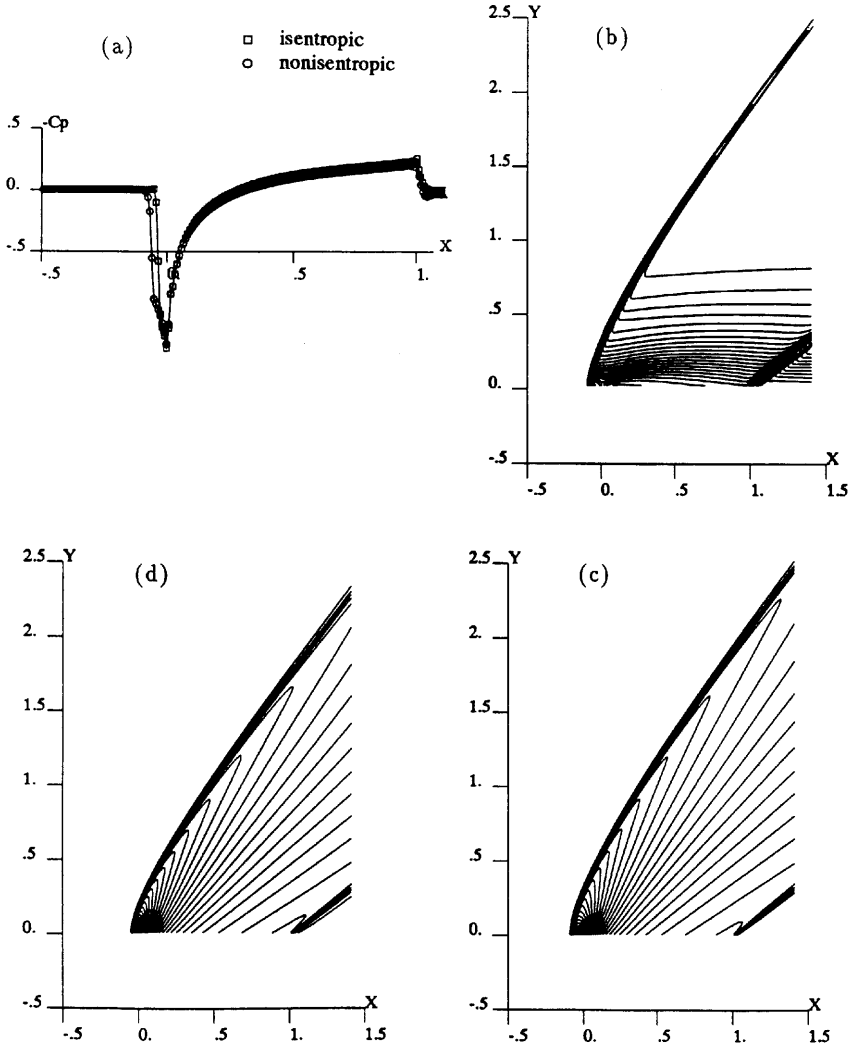

Figure 6. NACA 0012 aerofoil ($M_\infty = 1{\cdot}4$): (a) C_p distributions; (b) entropy contours; (c) pressure contours for non-isentropic flow; (d) pressure contours for isentropic flow

4. CONCLUDING REMARKS

The preliminary results are encouraging. Further studies are needed, however, to assess the merits and exploit the advantages of the present formulation.

ACKNOWLEDGEMENT

The results of the Appendix were calculated by C. Tang, a graduate student of UCD.

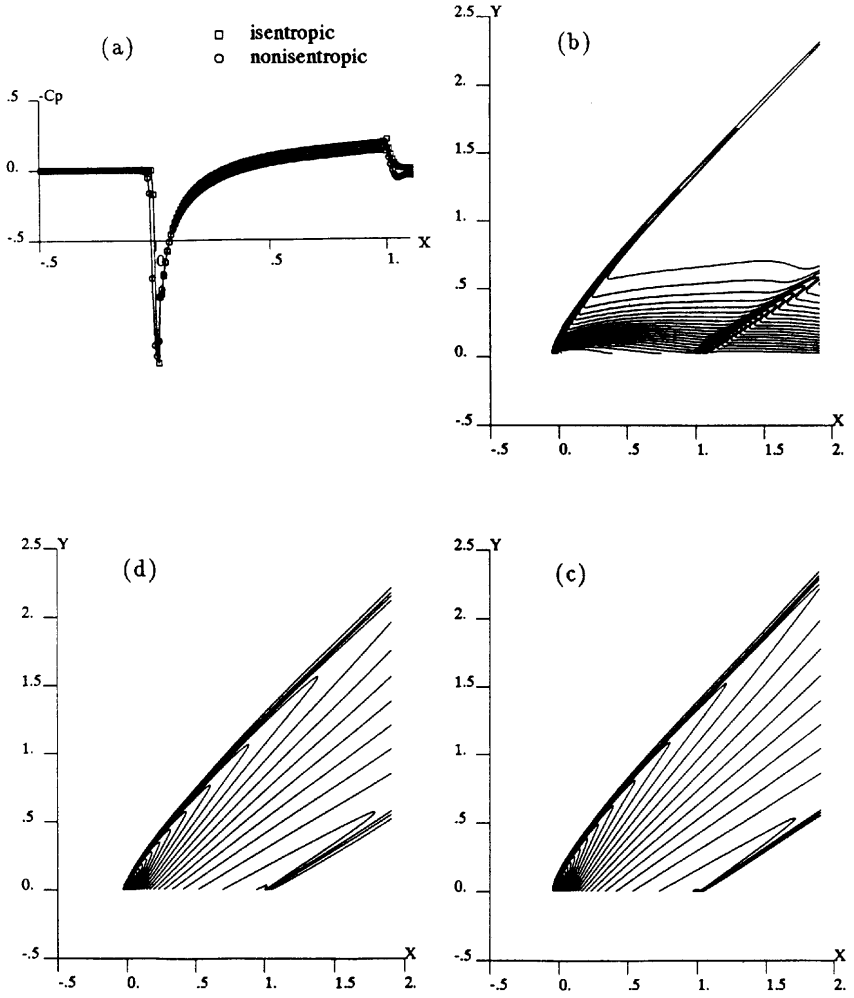

Figure 7. NACA 0012 aerofoil ($M_\infty = 1{\cdot}6$): (a) C_p distributions; (b) entropy contours; (c) pressure contours for non-isentropic flow; (d) pressure contours for isentropic flow

APPENDIX

Calculation of non-isentropic flows based on shock detection

Here the calculation of a non-isentropic flow based on the entropy generated across a shock wave is discussed. First the shock wave location and slope are detected, then the entropy jump is calculated in terms of the Mach number upstream of the shock. The distribution of the entropy downstream of the shock is obtained from the entropy transport equation. Hence the vorticity is evaluated using Crocco's relation. The Cauchy/Riemann equations are solved for the velocity components assuming the entropy and vorticity are known and the process is repeated until convergence.

The governing equations are

$$(\rho u)_x + (\rho v)_y = 0, \tag{16}$$

$$-u_y + v_x = \omega, \tag{17}$$

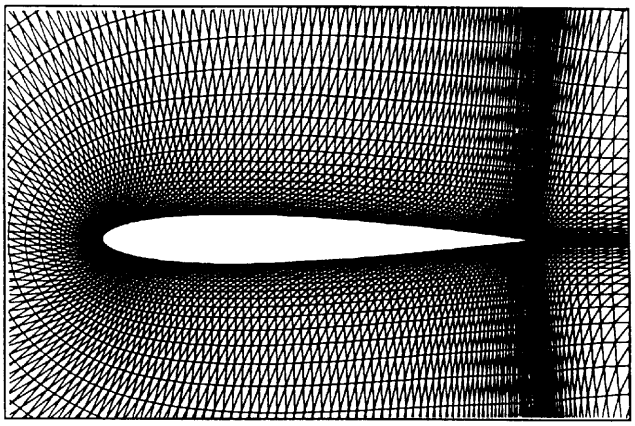

Figure 8. Grid for NACA 0012 aerofoil at zero angle of attack

where

$$\rho = \left(1 - \frac{\gamma - 1}{2} M_\infty^2 (u^2 + v^2 - 1)\right)^{1/(\gamma-1)} e^{-\Delta s/R},$$

$$\left(\rho u \frac{\Delta s}{R}\right)_x + \left(\rho v \frac{\Delta s}{R}\right)_y = 0, \tag{18}$$

$$\omega = \frac{p}{\rho q}\left(\frac{u}{q}\frac{\partial(\Delta s/R)}{\partial y} - \frac{v}{q}\frac{\partial(\Delta s/R)}{\partial x}\right). \tag{19}$$

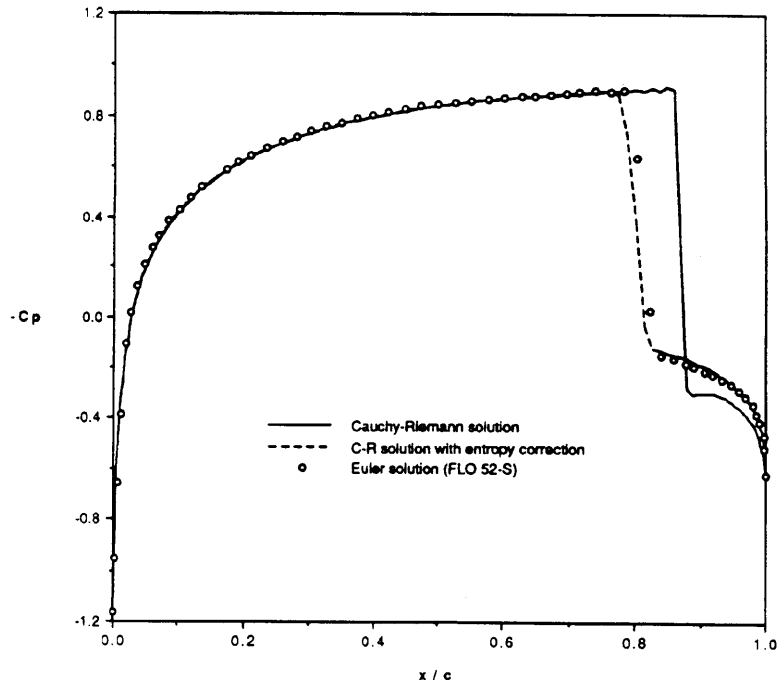

Figure 9. NACA 0012 aerofoil ($M_\infty = 0{\cdot}86$) C_p distribution

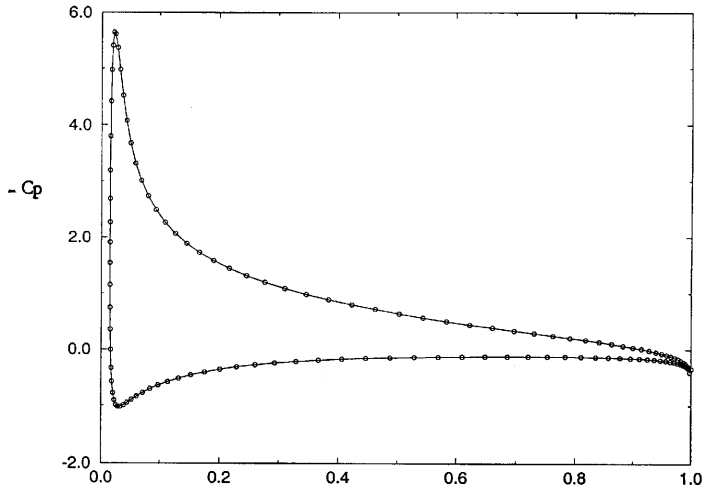

Figure 10. C_p distribution over NACA 0012 at 10° and $M_\infty = 0{\cdot}3$

Simulation of a transonic flow over an aerofoil using an artificial viscosity method and a finite element/finite volume discretization procedure over triangles similar to Reference 5 gives the results shown in Figure 9. The grid is shown in Figure 8. The result of the isentropic irrotational flow model ($s = \text{constant}$, $\omega = 0$) is compared with that of the non-isentropic rotational flow. The latter is in agreement with Jameson's FLO 52 calculations.

The problem of the shock detection, to calculate the boundary condition for the entropy equation, requires a special programming logic. Notice that entropy and vorticity are calculated only downstream of the shock, where they vary.

Calculations of subsonic lifting flows based on Cauchy/Riemann equations

For irrotational, isentropic flows the governing equations, conservation of mass and vorticity definition, are solved for the two velocity components, while the density is obtained from Bernoulli's law. On the differential level a potential function can be introduced and its gradient is the velocity

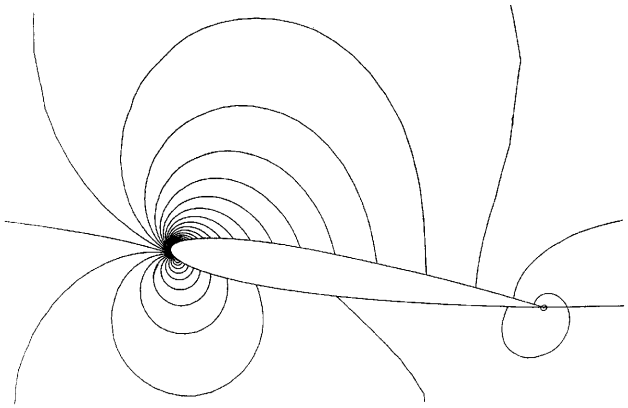

Figure 11. Mach number contours (levels vary from 0·025 to 0·9 with increments of 0·025)

vector. On the discrete level, however, a discrete potential may only exist for certain grids. In general, the difference between the discrete Cauchy/Riemann equations and the discrete potential equation is of the order of the truncaton error.

It is well known that a Kutta condition is necessary to solve the potential equation for lifting flows. For isentropic cases the flow should leave the aerofoil in the direction bisecting the trailing edge angle. Such a condition can be imposed explicitly in Euler calculations as well (see Reference 8 for more details). However, for the equivalent Cauchy/Riemann equations we will demonstrate that accurate solutions can be obtained using artificial viscosity methods as in standard Euler calculations. In Figure 10 the pressure distribution for an NACA 0012 aerofoil at 10° and $M_\infty = 0{\cdot}3$ is plotted. The agreement with the results of either FLO 36 or FLO 52-S of Reference 9 is excellent. The corresponding Mach number contours are plotted in Figure 11.

REFERENCES

1. A. Jameson, 'Artificial diffusion, upwind biasing, limiters and their effect on accuracy and multigrid convergence in transonic and hypersonic flows', *AIAA Paper 93-3359*, 1993.
2. P. L. Roe, 'Multidimensional upwinding: motivation and concepts', *VKILS 1994-05*, 1994.
3. M. Hafez and D. Lovell, 'Entropy and vorticity corrections for transonic flows', *AIAA Paper 83-1926*, 1983.
4. M. Hafez, 'Finite element/finite volume solutions of full potential, Euler, and Navier–Stokes equations for compressible and incompressible flows', *Int. j. numer. methods fluids*, **20**, 713–742 (1995).
5. C. Tang and M. Hafez, 'Finite element–finite volume simulations of viscous flows based on zonal Navier–Stokes equations—lifting transonic and supersonic flows', in *Solution Techniques for Large-Scale CFD Problems*, Wiley, New York, 1995.
6. H. Paillere, E. Vander Weide and H. Deconinck, 'Multidimensional upwind methods for inviscid and viscous compressible flows', *VKI Preprint 1995-12*, 1995.
7. S. Ta'asan, 'Essentially optimal multigrid method to steady-state Euler equations', *AIAA Paper 95-0209*, 1995.
8. R. Winterstein and M. Hafez, 'Euler solutions for blunt bodies using triangular meshes: artificial viscosity forms and numerical boundary conditions', *AIAA Paper 93-3333*, 1993.
9. M. D. Salas, A. Jameson and R. E. Melnik, 'A comparative study of the nonuniqueness problem of the potential equation', *AIAA Paper 83- 1888*, 1983.

